EUROFUSION WPJET1-PR(16) 14987

ER Solano et al.

Axisymmetric oscillations at L-H transitions in JET: M-mode

Preprint of Paper to be submitted for publication in Nuclear Fusion

This work has been carried out within the framework of the EUROfusion Consortium and has received funding from the Euratom research and training programme 2014-2018 under grant agreement No 633053. The views and opinions expressed herein do not necessarily reflect those of the European Commission.

Axisymmetric oscillations at L-H transitions in JET: M-mode

Emilia R Solano[1], N. Vianello[2], E. Delabie[3], J. Hillesheim[4], P. Buratti[5], D. Refy[6], I. Balboa[4], A. Boboc[4], R. Coelho[7], B. Sieglin[9], S. Silburn[4] , P. Drewelow[11], S. Devaux[8], D. Dodt[9], A. Figueiredo[7], L. Frassinetti[10], S. Marsen[11], L. Meneses[7], C.F. Maggi[4], J. Morris[4], S. Gerasimov[4], M. Baruzzo[12], D. Grist[4], I. Nunes[7], F. Rimini[4], I. Lupelli[4], C. Silva[6] and JET contributors[*]

EUROfusion Consortium, JET, Culham Science Centre, Abingdon, OX14 3DB, UK

[1]Laboratorio Nacional de Fusión, CIEMAT, Madrid, Spain; [2]EPFL-CRPP, Lausanne, Switzerland; [3]Oak Ridge National Laboratory, Oak Ridge, Tennessee, USA; [4]CCFE, Culham Science Centre, Abingdon; [5]UK Unità Tecnica Fusione - ENEA C. R. Frascati, Roma, Italy; [6]Wigner Research Center for Physics, Budapest, Hungary; [7]Instituto de Plasmas e Fusão Nuclear, IST, Lisbon, Portugal; [8]Institut Jean Lamour, CNRS-Université de Lorraine, France; [9]Max-Plank-Institut für Plasmaphysik, Garching, Germany; [10]Division of Fusion Plasma Physics, KTH Royal Institute of Technology, Stockholm SE; [11]Max-Plank-Institut für Plasmaphysik, Greifswald, Germany; [12]RFX, Corso Stati Uniti 4, Padova, Italy

E-mail: Emilia.Solano@ciemat.es

Abstract. L to H transition studies at JET have revealed an n=0 m=1 magnetic oscillation starting immediately at the L to H transition (called M-mode for brevity). While the oscillation is present a weak ELM-less H-mode regime is obtained, with a clear increase of density and a weak T_e pedestal, with medium confinement, between high (H-mode) and low (L-mode). In ICRH heated plasmas or low density NBI plasmas the mode and the pedestal pressure can remain steady for the duration of the heating phase, of order 10 s or more. The axisymmetric magnetic oscillation has period ~ 1-2 ms, and poloidal mode number m=1: it looks like a pedestal localised up/down oscillation, although it is clearly a natural oscillation of the plasma, not driven by the position control system. Electron Cyclotron Emission, interferometry, reflectometry and fast Li beam measurements locate the mode in the pedestal region. D_α, fast infrared camera and Langmuir probe measurements show that the mode modulates heat and particle flux to the target. The mode frequency appears to scale with the poloidal Alfvén velocity, and not with sound speed (i.e., it is not a Geodesic Acoustic Mode). A heuristic model is proposed for the frequency scaling of the mode. We discuss the relationship between M-mode and other related observations near the L-H transition.

PACS: 52.55.Fa, 52.35.Py, 52.35.Vd

1. Introduction and general description of M-mode

Experimental studies of L-H transitions in JET in 2011 [1] have rediscovered a low frequency n=0, m=1 coherent magnetic oscillation starting immediately at the transition (named M-mode at JET for brevity) [2, 3, 4]. Corresponding oscillations are clearly observed in many pedestal and SOL diagnostics, particularly in D_α emission from the divertor. While this oscillation is present a weak ELM-less H-mode regime is obtained (with medium confinement, hence the name), with a clear increase of density and a weak T_e pedestal. In Ion Cyclotron heated (ICRH) plasmas or low power, low density Neutral Beam Injection (NBI) heated plasmas the M-mode oscillation and the pedestal pressure can remain steady for the duration of the heating phase, of order 10 s or more. Data mining of all slow historical L-H transitions in JET has revealed that the M-mode was present in all cases in the relevant magnetic measurements, if sufficient acquisition rates were available: Carbon-wall, ITER-

[*] See the Appendix of F. Romanelli et al., Proceedings of the 25th IAEA Fusion Energy Conference 2014, Saint Petersburg, Russia

Like-wall, various isotopes: Hydrogen, Deuterium, Tritium, Helium..

The observed axisymmetric magnetic oscillation has a period of order 1-2 ms, and odd parity across the mid-plane: it is equivalent to an up-down oscillation of the plasma, n=0, m=1, $\propto \sin(\theta)$. The M-mode frequency is not associated with plasma toroidal rotation, nor is it due to the vertical position control system. See Section 3 for details.

The M-mode is detected as well in pedestal and SOL measurements. Electron Cyclotron Emission, SXR, interferometry, reflectometry and fast Li beam measurements detect and localise the M-mode in the upper pedestal. D_α, fast infrared camera and Langmuir probe measurements in the divertor show oscillation of heat and particle flux to the target. See detailed description in Section 4.

Shown in Figs 1 and 2 are some of the most salient characteristics of the M-mode: as usual the L-H transition is marked by a drop in D_α. We show that simultaneously a mode appears in the Fast Fourier Transform (FFT) of a poloidal Mirnov coil located in the plasma high field side (HFS), half-way above the midplane. Further, the FFT of a fast electron cyclotron emission channel in the plasma pedestal indicates pedestal localisation, corroborated by reflectometry and Beam Emission Spectroscopy (not shown in these figures). Fig. 2 illustrates profile evolution, showing an increase in the density at the pedestal top, and formation of a weak electron temperature pedestal. Averaged over

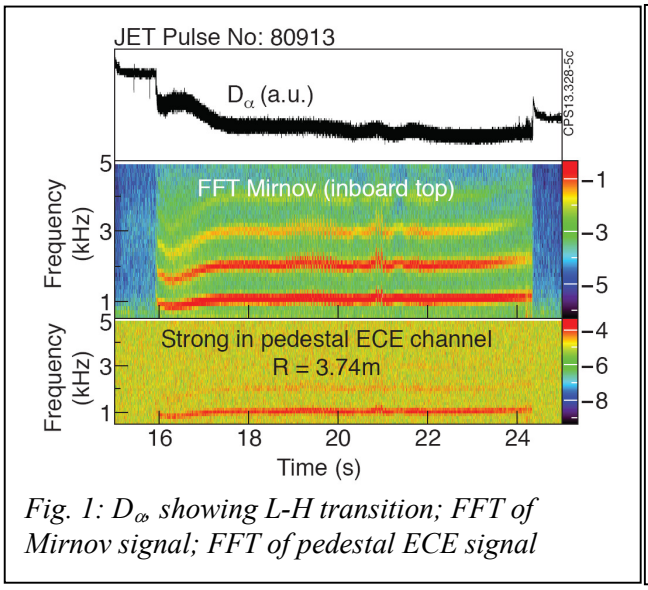

Fig. 1: D_α, showing L-H transition; FFT of Mirnov signal; FFT of pedestal ECE signal

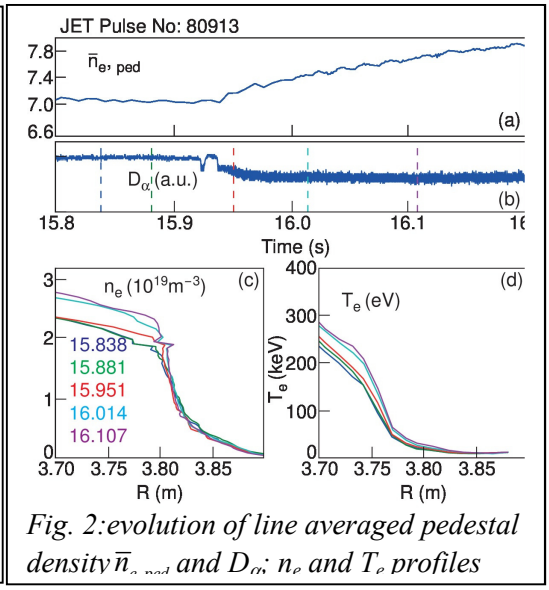

Fig. 2:evolution of line averaged pedestal density $\bar{n}_{e,\,ped}$ and D_α; n_e and T_e profiles

the oscillation's period, confinement is "medium": better than in the preceding L-mode, worse than in ELM-free or type I ELMy H-mode.

The M-mode is clearly magnetic in character and we will show that its frequency appears to scale with the local poloidal Alfvén speed, $\propto I_p/\sqrt{(m_i\, n_e)}$ (I_p is plasma current, n_e is electron density, m_i the ion mass). Generally mode frequency does not scale with electron temperature: it is not a Geodesic Acoustic Mode (GAM). Scaling of mode frequency will be discussed in Section 4, including a heuristic theoretical model for it.

Similar phenomena have been reported and discussed at JET and elsewhere [2, 5-20], usually concentrating on electrostatic fluctuation measurements in similar frequency ranges. This is a rapidly advancing field, references [5-21] may not include all the latest or relevant results, but are representative. Reference [20] presents a good global view of previous studies. The many observations reported are variously described as L-H dithering transitions, Limit Cycle Oscillations or small ELMs. Limit Cycle Oscillations are usually explained in terms of a complex interaction between zonal flows, Geodesic Acoustic Modes (GAMs), electrostatic turbulence, radial electric fields (E_r) and mean flows, cast in a number of predator-prey models. Articles often mix observation with theory-based models. To our knowledge none of those turbulence and transport-related views of the L-H oscillations would lead to a ~1 kHz up-down magnetic oscillation with frequency proportional to $I_p/\sqrt{(m_i\, n_e)}$ We will

discuss these and other related observations in Section 5.

2. Magnetic characteristics of the M-mode

Shown in Fig. 3 are the signals from Mirnov coils distributed toroidally around the tokamak, located poloidally half-way above the plasma equator, in the low field side. It is evident that the magnetic oscillations are in phase: the mode is axisymmetric, n=0. Therefore it should not be surprising that mode frequency is unrelated to plasma toroidal rotation: the magnetic oscillation is simultaneous in all coils of the toroidal array, it is not due to a toroidally travelling pulse.

Shown in Fig. 4 are the signals from the poloidal arrays (all except one smoothed in time to eliminate oscillations faster than 100 kHz), showing that the M-mode magnetic oscillation is proportional to sin(θ): i.e., magnetically similar to very small up-down displacements of the plasma (sub-millimiter). The mode amplitude is so low near the plasma equator that an FFT of equatorial Mirnov measurements would not pick up the M-mode. We suspect this is why similar modes have been labelled as "non-magnetic" in other studies/devices, see section 5.

When the M-mode is sufficiently strong the adaptive vertical position control system [22,23] detects a displacement of the current centroid and sometimes it reacts to it, as shown in the bottom 3 traces of Fig. 4. There are many periods of time when the mode is not coupled to the position control system, while in other cases each oscillation elicits a response. Only when the M-mode amplitude is large and its frequency low, below 700 Hz, the adaptive plasma position control system interacts with it in most

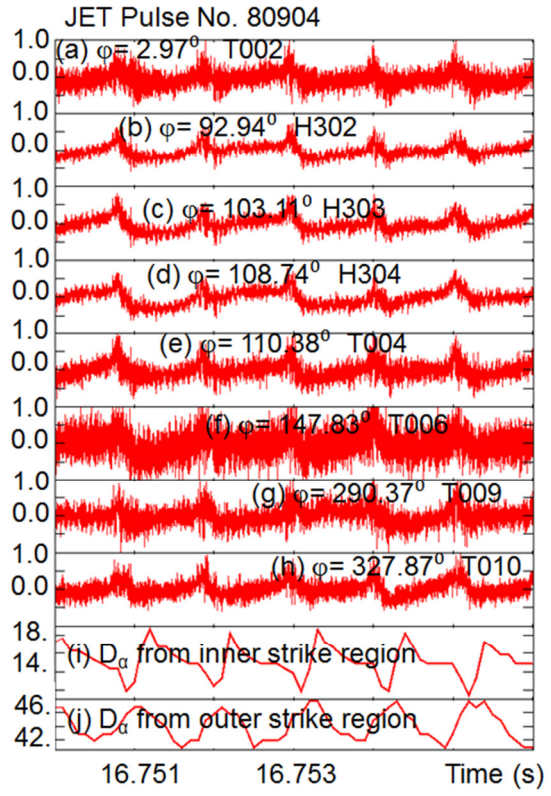

Fig. 3: a-h) Mirnov signals from toroidal array, dB_θ in T/s, showing mode is axisymmetric, simultaneous at all toroidal locations, n=0; global D_α from (i) inner and (j) outer strike region (in photons/cm^2/sr)

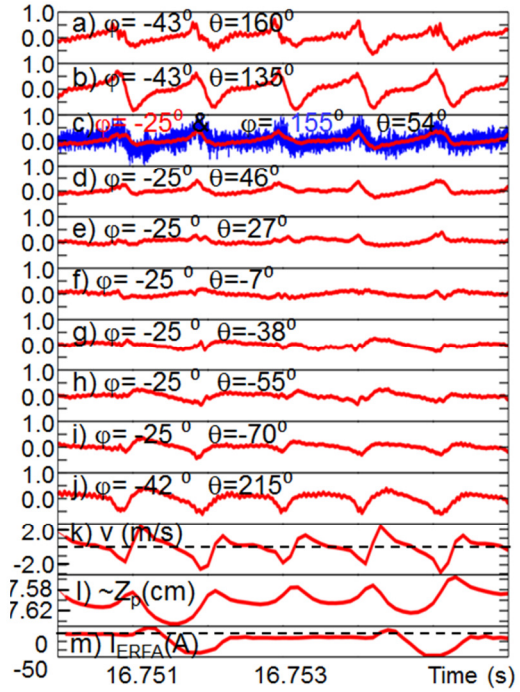

Fig.4: a-j) Mirnov signals (time smoothed every 10 samples) of poloidal array (unsmoothed signal at different toroidal location shown in blue in c) for comparison; k) plasma velocity proxy, used for position control; l) vertical current centroid proxy; m) current in vertical position control supply, showing reaction of system for two cycles of M-mode

cycles. In any case the plasma current centroid displacement due to the M-mode is sub-mm. Careful analysis of a variety of cases shows that the apparent up-down magnetic oscillation is not always centred at the height of the plasma magnetic axis, but can also be displaced towards the X-point (downwards) by about 10 cm.

Note that in JET the MHD Mirnov sensors measure dominantly poloidal field oscillations, not radial. In other devices, notably ASDEX and ASDEX-Upgrade, MHD studies were usually made with measurement of oscillations in the radial component of the field, B_r. High field side coils are much less affected by sawteeth precursors and other core MHD modes that often have similar frequencies to the M-mode at JET. This is why we find that M-mode identification is best done in the spectrogram of an off-axis HFS Mirnov.

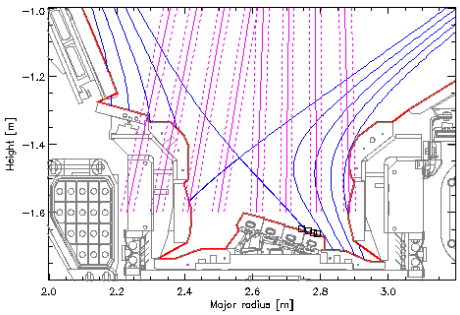

Fig. 5: Representative lines of sight of D_α views at inner and outer strike locations, and positions of Langmuir probes, used for plots of Figs.6,7. The R coordinate shown in Fig. 6 for D_α corresponds to the lowest point in each channel.

Further we should mention that the MHD Mirnov sensors at JET are suffering from high attrition since 2012, so the more recent the pulse, the less information is available about mode geometry. Generally we can still determine if n=0, and if the mode is up-down symmetric.

3. M-mode in Pedestal and SOL measurements:

As well as in the magnetics, M-mode oscillations are often very clear in the D_α light emitted from both inner and outer strike regions, with the peculiarity that inner and outer photon global fluxes often oscillate out of phase. Shown in Fig 5 is the diagnostic set-up for visible spectroscopy and Langmuir probes. Additionally an infra-red camera is used to measure temperatures and derived heat fluxes in the outer strike region.

In Fig. 6 we show M-mode oscillations of outer target heat flux (measured with an Infra-red camera),

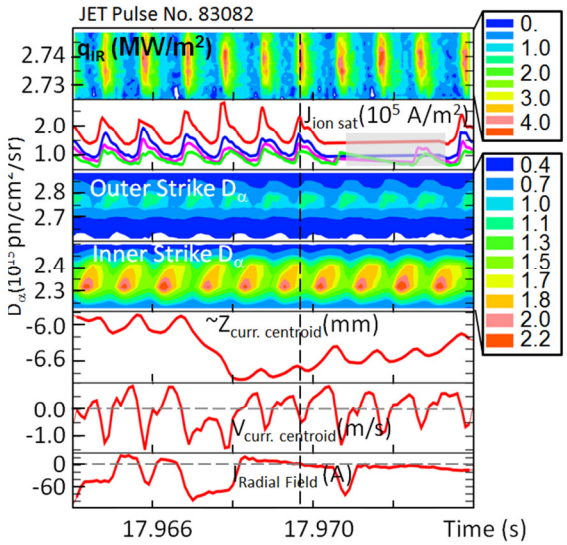

Fig. 6: a) Outer target heat flux profiles(IR measurement); b) Ion saturation current at outer strike (red) and progressively further out; c,d) D_α profiles at outer and inner strikes e) plasma vertical position proxy, f) Plasma velocity proxy, used for position control (dashed lines mark zero); g) current in vertical position control power supply (dashed lines mark zero).

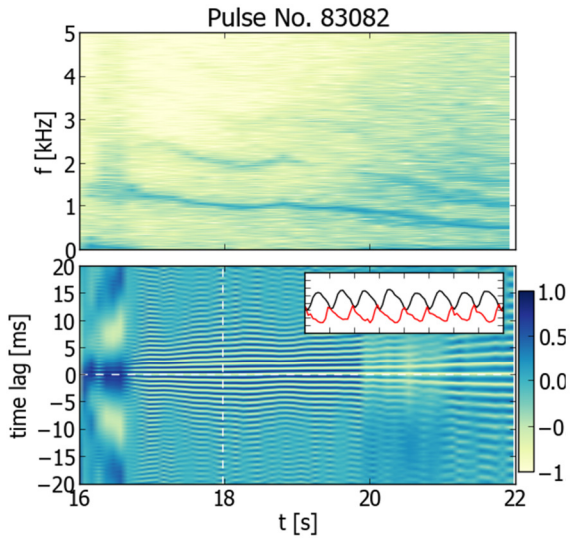

Fig. 7: a) spectrogram from D_α emission at the inner divertor showing M-Mode from ~16.3 s. b) Cross-correlation between inner and outer divertor D_α emission, where the anti-correlation can be recognized. In the inset the time traces of inner (black) and outer (red) divertor emission in a small time window around the marked vertical position

ion saturation current at outer strike from Langmuir probes (the shaded area in this data is due to the voltage sweep, when ion saturation current is not being measured) and profiles of line integrated D_α light, both outboard and inboard. Taken together this indicates the simultaneous arrival of bursts of heat and particles at the outer strike. Also shown in Fig 6 is a plasma vertical position proxy derived from the vertical position control signals, as well as the proxy for the vertical velocity of the current centroid, positive for upwards motion of the plasma. Also the current driven in the radial field supply to compensate detected motion is displayed. In this example we can see that periodic releases of particles and energy take place when the plasma is at the top of its up-down oscillation, or soon afterwards. As the plasma "moves down" the SOL widens and a pulse of heat, ion saturation current and particles is seen, without displacement of the strike point. As the plasma moves up from its bottom position the outward particle and heat fluxes are minimum. We also see again that the mode is not driven by the position control system, which in this case only acts on the plasma in about half of the cycles.

Asshown in Fig. 6.d, D_α emission in the inner strike region is maximum at the 1 cm SOL line, quite high above the inner strike (the second channel from the left shown in Fig. 5). The maxima in inboard light are generally out of phase with the maxima of the outboard light. It is likely that the plasma is partially detached on the inboard, near the recombination regime. In that case the arrival of heat would produce a reduction in inboard D_α emission from the far SOL, as observed. A correlation analysis between inner and outer D_α is shown in Fig. 7. In the top panel we show a spectrogram of summed D_α light from the inner strike viewing channels, where the M-Mode is clearly observable from 16.3 s. In the bottom panel we show the cross-correlation between inner and outer strike light emission as a function of time and lag. A sharp transition is clearly identified whenever the M-mode appears. Also shown in the zoom in the inset, is a detail of global inner and outer divertor D_α light oscillations. This D_α behaviour is not always present. For instance there are cases in low density Carbon-wall pulses when the inboard divertor is attached and D_α signals inboard and outboard are in phase.

The M-Mode is clearly detected as a fluctuation of pedestal density. Shown in Fig 8 are some reflectometer measurements: a) the estimated radial displacement associated with the mode, along the reflectometer line of sight close to the outer midplane, and b) the corresponding density profile, averaged during the same time period of t=19-20s. The displacement is estimated as the RMS

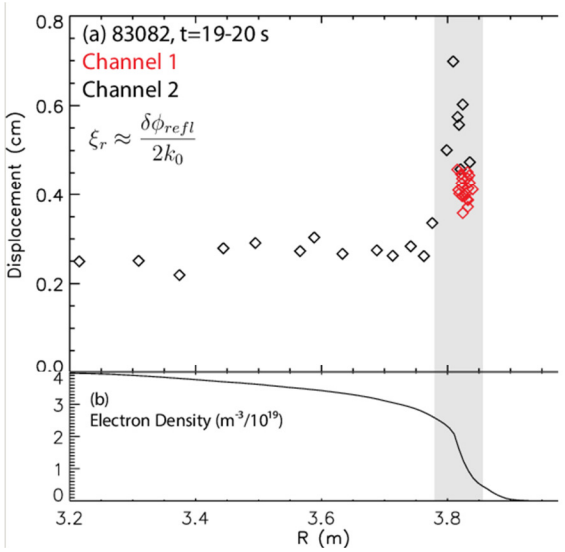

Fig. 8: (a) estimated radial displacement from correlation reflectometry measurements in outer midplane, as a function of major radius; (b) electrin density profile, measured by profile reflectometer.

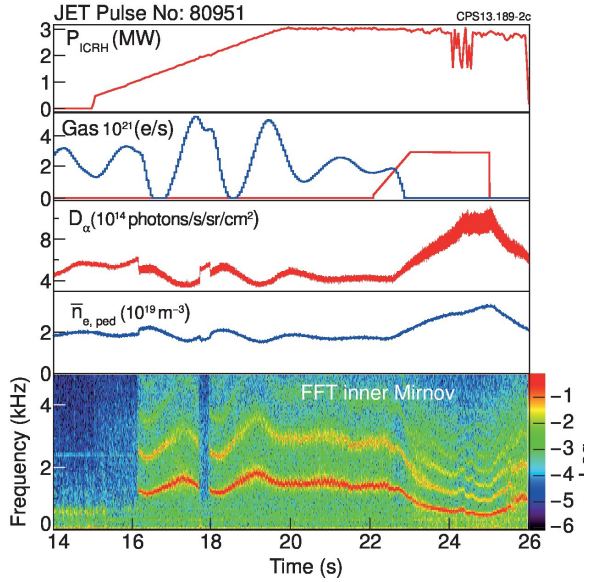

Fig. 9: evolution of auxiliary heating, fuelling (blue for feedaback, red for extra), D_α, $\bar{n}_{e,ped}$ and mode frequency

reflectometer phase fluctuation, bandpass filtered around the M-mode frequency, divided by 2 times the vacuum wavenumber. The RMS phase fluctuation is determined by averaging over 20 different 50 ms time periods for each channel between t=19-20 s, as the reflectometer frequency was scanned to change the measurement radius (each radial point is 50 ms). There is a background level, as can be seen from the core data points, but where the M-mode is clearly visible in the spectrogram, it is up to 5 mm above the background. From this we conclude that the M-mode is clearly localised in the pedestal of the density profile. This pedestal localisation has been independently determined by analysis of Beam Emission Spectroscopy from the Li-Beam diagnostic. Both the density and the density gradient show an oscillation at M-mode frequency [4] and the data is compatible with a combination of small plasma up-down motion and a periodic change in the density gradient in the pedestal region. Note that the BES system at JET views the top of the plasma, not the outer equator. The phase information on density (BES) vs. temperature (ECE, outer equator) oscillations is inconclusive. Present data are not sufficient to provide a clear statement on pressure profile oscillations and further analysis with improved diagnostic capabilities are foreseen for the forthcoming campaign.

During the M mode the pedestal density responds to changes in fuelling more readily than in ELMy H-mode: increased fuelling leads to increased density. This indicates that the improvement in particle confinement is not counter-acted by the periodic particle losses detected in the SOL. In conventional type I regimes plasma density is rarely controlled by fuelling, because as fuelling increases ELM frequency and particle losses increase. As shown in Fig. 9 during the M-mode a rise in density, due to a deliberate increase in fuelling, leads to a drop in M-mode frequency. Note that the delay in the density rise after the increase in fuelling at 22 s is due to the long distance between the Deuterium injection valve and the plasma.

4. Scaling of M-mode frequency

Natural density evolution after the L-H transition correlates clearly with mode frequency, and a comparison of otherwise similar plasmas at different current show that mode frequency is also related to plasma current. The best ordering of M-mode frequency is given by the poloidal Alfvén velocity at the pedestal top, $V_{Alfvén,\theta} = B_\theta / \sqrt{\mu_0 m_i n_i}$. Here m_i is the ion mass, n_i the ion density and B_θ the poloidal field. For simplicity $V_{Alfvén,\theta}$ is calculated assuming the pedestal is at 97% of the normalised poloidal flux, the poloidal field is flux surface averaged and ion density is assumed equal to electron density, which is measured as a vertical line average across a typical pedestal location. Shown in Fig. 10 is the

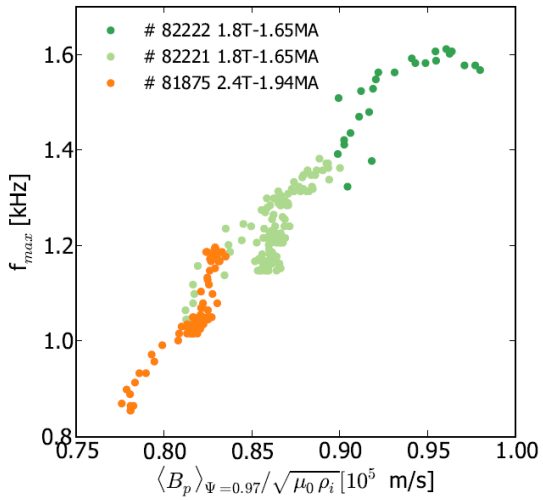

Fig. 10: Plot of $V_{Alfvén,\theta}$ vs. measured M-mode frequency for time-varying M-modes in RF heated plasmas.

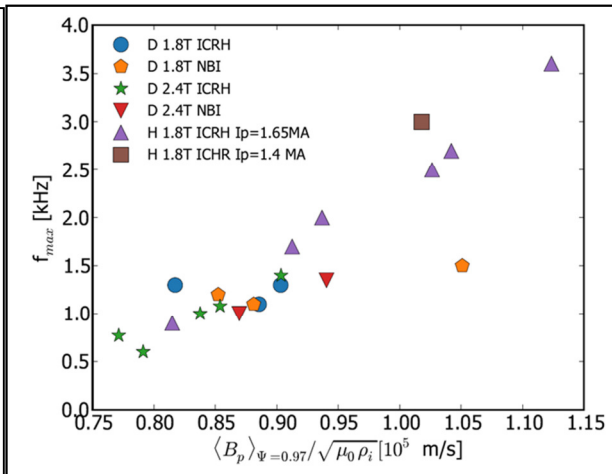

Fig. 11: mode frequency as a function of $V_{Alfvén,\theta}$ for steady phases of various Deuterium and Hydrogen plasmas, and various shapes, with different auxiliary heating, current, density.

time-varying mode frequency represented against $V_{Alfvén,\theta}$ for ICRH plasmas with the same shape but different current and field. There are no adjustable parameters in the plot: the trend is very clear.

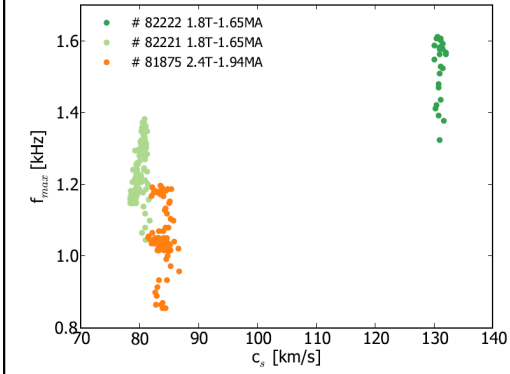

Fig. 12: mode frequency as a function of ion sound speed, for same plasmas shown in Fig. 11

To further investigate mode frequency scaling we have compiled a database of various slow L-H transitions in pulses with varying input power, ICR and NBI heating, density, current, toroidal field, plasma shapes, both in Hydrogen and Deuterium. The characteristic frequency was chosen in a time window where the mode is steady and the control system misses at least 6 consecutive M-mode cycles. In most cases with frequencies below ~700 Hz the plasma position vertical control system responds to every M-mode oscillation, possibly affecting what might be the natural mode frequency. In fact when we look at the time variation of mode frequency within a pulse we observe a linear trend as in Fig 10, regardless of whether the control system is involved.

Returning to the overall trend and Fig. 11: the database confirms the connection between mode frequency and poloidal Alfvén velocity, particularly for ICRH heated plasmas. The slope looks steeper in Hydrogen than in Deuterium plasmas, and NBI heated plasmas deviate from the trend. There are very few NBI heated data points, and their intrinsic particle fuelling leads to large densities, unsteady mode frequencies and quick transitions to a mixed M-mode/type III regime (see next section). Hopefully future studies will be able to ascertain the reason for this deviation from the scaling observed in RF heated plasmas.

Shown in Fig. 12 is the lack of correlation between mode frequency and ion sound speed at the pedestal for the same pulses as in Fig. 11. This excludes the initial hypothesis that the M-mode is related to a type of GAM.

There many other global variables unrelated to mode frequency: toroidal magnetic field, heating power, beta poloidal, core density, etc.

We are not aware of any theoretical model that relates poloidal Alfvén frequency with the L-H transition, nor with any stationary MHD wave. We consider it likely that an axisymmetric MHD mode will not be associated with the total or toroidal magnetic field, but with the poloidal field, because Alfvén waves are driven by $\vec{k}\cdot\vec{B}$ ($\vec{k}$ is the wave vector of the mode). Since there is no wave propagation in the toroidal direction, $k_{||}$ only has a poloidal component. But this is not just a conventional surface Alfvén wave propagating along the field line, where $k_{||}$ would need to be of order 10^3 m^{-1} to match the mode frequency. It is actually similar to a hydrodynamic surface wave, as described in textbooks [24], with the driving term being the magnetic tension instead of the density gradient. Proceeding by analogy, the relation between wave frequency and velocity in a slab model with x in the radial direction and y in the poloidal direction would be:

$$\omega^2 = \kappa_y^4 V_{Alfvén,y}^2 \Big/ \left(\kappa_x^2 + \kappa_y^2\right) \simeq \kappa_y^4 V_{Alfvén,y}^2 \Big/ \kappa_x^2 \Rightarrow \nu = \frac{\omega}{2\pi} \simeq \frac{\lambda_r V_{Alfvén,\theta}}{2\pi L_\theta^2} \qquad (1)$$

Here k_x, k_y would be the x and y components of the wave vector, mapped to radial and poloidal k_r, k_θ in a cylindrical model. Equivalently λ_r and λ_θ are radial and poloidal scale lengths. Because the mode has m=1, λ_θ is the plasma perimeter, while λ_r would be the radial scale length of the mode.

If the dispersion relation (1) is correct, it could match the plots in Fig. 11 and 12 for radial scale lengths of the mode order ~1 cm, and might explain the different slopes for Hydrogen and Deuterium if their density gradient lengths are different. The density scale length in the pedestal region is not easy to evaluate, but it is compatible, in M-mode, with such numbers. Forthcoming studies of L-H transitions at JET with enhanced reflectometry measurements and interpretation may allow us to investigate this further. Equation (1) might also explain why plasma shape affects mode frequency (via the poloidal length), and might even lead to quantised allowed frequencies for fixed density, since the mode would be effectively a poloidal standing wave. In a few pulses we have observed step changes in frequency by a factor of 2.

So far we have been unable to derive the dispersion relation (1) correctly in the context of MHD theory in a cylindrical or toroidal plasma. A possible MHD mode that might exhibit the $1/\sqrt{(m_i n_e)}$ aspect of the frequency scaling may be an interchange or Mercier poloidally standing wave, possibly driven by plasma magnetisation instead of curvature, as described in [25], but it is not clear why plasma current should appear in the scaling in that case.

5. Other observations near the L-H transition: dithering, GAMs, other devices

The dynamics of the L-H transition at JET are described in [25], including a detailed discussion of divertor oscillations [26], which sometimes precede the transition, and the correlation between divertor oscillations and dithering transitions between L and H phases. Here we would like to illustrate the different stages between L-mode and ELMy H-mode.

A global view of an L-H transition in an NBI heated pulse is shown in Fig. 13, displaying a dithering phase (pedestal density stays low), the M-mode (with increase of pedestal density), a mixed phase with some type III ELMs and an ELM-free phase followed by a type I ELM, Time zooms are shown in Fig. 14. The figures show that the M-mode is already present during the high confinement phase of the low frequency dithers. The IR measurement of temperature maximum as a function of time in the outer strike region indicates larger heat fluxes during the L-phase of the dithers, as well as in the periodic bursts of the M-mode oscillations. In Fig. 14-Right type III ELMs are clearly visible, especially in the D_α emission intensity from further out in the SOL, and in T_{IR}.

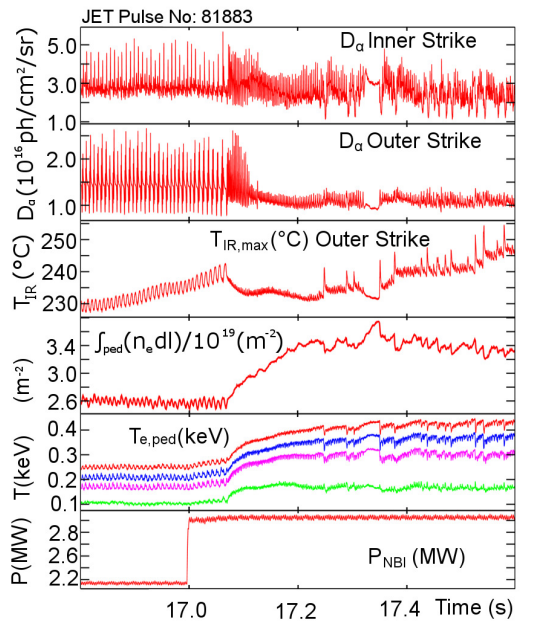

Fig. 13: Da emission from a) inner and b) outer strike; c)maximum T_{IR}; d) line integral of $n_{e,ped}$; e) $T_{e,ped}$ and f) NBI input power.

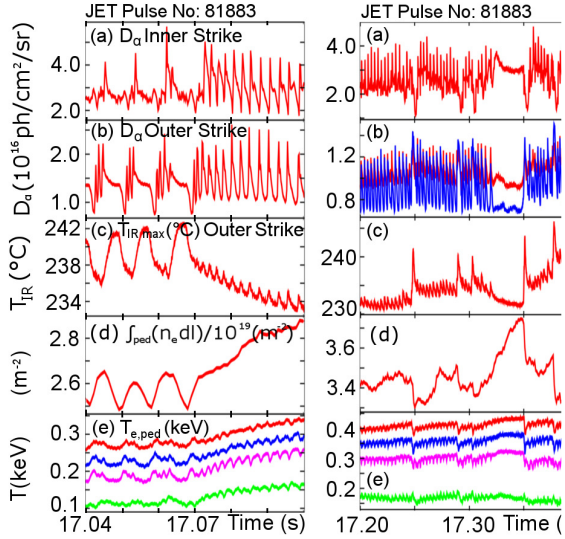

Fig. 14: Left: Zoom of Fig 14 showing 3 L-H dithers and the M-mode phase. Right: M-mode phase with type III ELMs and one ELM-free period followed by a type I ELM. Blue line in b) is D_α at far outer SOL.

The above sequence of events has been observed and reported in various devices and there has been much debate on nomenclature. Zohm reported "dithering transitions" and identified them as "Limit Cycle Oscillations" in ASDEX [6]. DIII-D described both type IV ELMs [27] and a predator-prey instability detected in the "IM mode" [7]. Both appear to share characteristics with the JET M-mode. The IM-mode is an intermediate phase between L and H-mode, seen in slow L-H transitions. Interestingly in the DIII-D IM-mode $T_{e,ped}$ is reported to improve while $n_{e,ped}$ remains clamped. In JET we observe a stronger increase in $n_{e,ped}$ than in $T_{e,ped}$ during the M-phase. At JET the M-mode was first described as "transition ELMs" in pulses from the DT campaign [2, unpublished]. This study is only available as an internal report, and was forgotten by many until recently. In most of the older studies (with the exception of JET) the modes were declared as non-magnetic because they were not seen (or only weakly) in Mirnov coils located at the outer plasma equator. At the time prevalent theories of ELMs pointed towards ballooning modes as explanations, so off-equator measurements were either not available or not considered.

More recently the I-phase has been described in the TJ-II stellarator [8] and at AUG [9]. Observations are cast as LCOs from interaction of predator-prey type in electrostatic turbulence and transport models. Even more recently low frequency coherent magnetic oscillation appearing in conjunction with pedestal and edge fluctuations have been reported around the L-H transition in EAST [15, 17, 20], HL-2A [18], JFT-2M [19] and AUG [21], clearly identified as n=0 and m=1 in [20,21].

Numerous theoretical and modelling studies are available on Limit Cycle Oscillations as explanations for either ELMs or dithering transitions [5,6,10,13]. Generally the interpretations focus on Limit Cycle Oscillations in predator-prey electrostatic turbulence and transport models: a complex interaction between zonal flows, E_r, turbulence, GAMs, Reynolds stress, mean flows and transport. All of these models have in common the fact that they describe n=0, m=0 changes in pedestal characteristics, and do not explain why n=0, m=1 up-down magnetic oscillations should be present. Therefore it is unlikely that these models will explain the M-mode.

Initially it was assumed that the M-mode observed at JET is the same phenomenon then described in AUG as an I-phase. At the time the I-phase had been characterised as not having a magnetic component [9]. The I-phase experts consulted then would not accept that the JET M-mode was an I-phase unless we provided data on the interactions between GAMs, zonal flows and E_r in the JET observations. Lacking the necessary diagnostics, we had to create a new name, and because the mode was clearly magnetic and plasma confinement was medium, we chose M-mode. More recently it is now believed that the I-phase of AUG is likely to correspond to the the JET M-mode [21], although some joint studies may be necessary to clarify the situation. It is possible that further subdivisions will appear as we bring more attention to these transitions, and more diagnostics become available..

Magnetic modes with n=0 and frequencies of order 10-15 kHz have been identified as GAMs in JET [29]. Magnetic oscillations in the 8-15 kHz frequency range with n=0 are often seen in the L-mode phase preceding the transition, during the L-phase of the low frequency dithering transitions.

In some cases (but not all) n=1 magnetic modes in the 20 kHz range are intermittently or continuously present during the M-phase, and can exhibit sidebands separated by the M-mode frequency. Their magnetic signatures are too weak to allow us to establish if the amplitude of these modes is modulated by the M-mode. Planned experiments at JET with better diagnostics may shed light on the precise nature of the M-mode and its interplay with GAMs, other MHD modes and electrostatic turbulence.

In any case, it is worth noting that M-modes are likely to be present in any power-starved plasma, such as in ITER. It would be useful to know more about their confinement characteristics, and whether they can modify the power required to enter the type III and type I ELMy regimes, which have hotter pedestal and, due to stiffness, better confinement.

6. Summary and open questions

We described the JET M-mode, an n=0, m=1 magnetic mode correlated with a series of periodic plasma expulsions detected with SOL diagnostics. The mode is located in the region of the density pedestal knee and high gradient region. It is present in all slow L-H transitions, while power and density remain near the L-H transition threshold values. Its frequency is given by an Alfvén-type relation.

Although the Limit Cycle Oscillations of predator-prey models are very popular explanations of the variously named versions of this or similar modes observed at the L-H transition, it should be said that LCOs are by definition n=0, m=0, without change of plasma equilibrium. To our knowledge no explanation has yet been advanced for the strong magnetic signatures observed, or for the n=0, m=1 magnetic up-down oscillation. And why would such a "limit cycle" have a frequency related to the poloidal Alfvén velocity?

Acknowledgements:

Ernesto Lerche, Dirk van Eester, Philipe Jacquet, George Sips and Giuseppe Calabro have provided us with opportunities to study the M-mode in their experiments, and/or helped us obtain useful plasmas. Agatha Czarneka and Dirk van Eester did some early data analysis to show the mode had no special characteristics due to impurities or RF effects. We have had interesting discussions with Jon Graves, Xavier Garbet, Gregori Birkenmeier, Garrard Conway, Teresa Estrada, Guo-Shen Xu, both about the nature of GAMs and LCOs and similarities/differences in similar modes in other devices.

This work has been carried out within the framework of the EUROfusion Consortium and has received funding from the EURATOM research and training programme 2014-2018 under grant agreement No 633053. The views and opinions expressed herein do not necessarily reflect those of the European Commission.

References:

1. C. Maggi et al, 39th EPS Conf. on Plasma Physics & 16th ICPP, Stockholm, Sweden, 2012 O3.108 and CF Maggi, et al, Nucl. Fusion 54 023007 (2014)

2. Chankin et al, ELM Activity in "Dithering" L-H Transitions on JET (1997), JET-P(97)23, http://www.euro-fusionscipub.org/wp-content/uploads/2014/11/JETP97023.pdf

3. E. R. Solano et al, 40th EPS conference on Plasma Physics, Espoo, Finland, 2013, Poster P4.111, http://ocs.ciemat.es/EPS2013PAP/pdf/P4.111.pdf

4. N. Vianello et al, 42nd EPS Conference on Plasma Physics, Lisbon, Portugal (2015), P2.133 http://ocs.ciemat.es/EPS2015PAP/pdf/P2.133.pdf

5. S. Itoh et al, Phys. Rev. Lett. 67 (1991)

6. H. Zohm Phys. Rev. Letts. 72 (1994)

7. D. Colchin et al, Phys. Rev. Letts. 88 (2002)

8. T. Estrada et al, EPL 92, 35001 (2010)

9. G. Conway et al., Phys Rev. Letts. 106, 065001 (2011)

10. D. Constantinescu et al, Phys. Plasmas 18, 062307 (2011) http://dx.doi.org/10.1063/1.3600209

11. G. S. Xu, Phys. Rev. Lett. 107, 125001 (2011)

12. T. Estrada et al., Phys. Rev. Letts. 107, 245004 (2011)

13. K. Miki et al, Physics of Plasmas 19, (2012), http://dx.doi.org/10.1063/1.4753931

14. G.S. Xu et al, Phys. Plasmas 19, 122502 (2012); http://dx.doi.org/10.1063/1.4769852

15. H. Q. Wang NF 2012; Phys. Plasmas 21, 092511 (2014); http://dx.doi.org/10.1063/1.4896237

16. L. Schmitz et al., Phys. Rev. Lett. 108, 155002 (04/2012)

17. T. Zhang, Phys. Letts. A (2013)

18. J. Cheng, Phys. Rev. Lett. 110, 265002 (2013)

19. T. Kobayashi et al, Nucl. Fusion 54 (2014) 073017

20. G. S. Xu et al, Nucl. Fusion 54, 103002 (2014)

21. G. Birkenmeier et al, 42nd EPS Conference on Plasma Physics, Lisbon, Portigal (2015) http://ocs.ciemat.es/EPS2015PAP/pdf/P1.125.pdf

22. M. Lennholm et al. Plasma control at JET, Fusion Engineering and Design 48 (2000) 37–45

23. F.G. Rimini et al, Fusion Engineering and Design 86 (2011) 539–543.

24. D. J. Tritton, "Physical Fluid Dynamics", 2nd Edition, Oxford Univ. Press (1998), equation (15.37)

25. E. R. Solano & R. D. Hazeltine, Nucl. Fusion 52 114017 (October 2012)

26. E. Delabie et al, 25th IAEA Fusion Energy Conference Proceedings, 13-18 October 2014, St. Petersburg, Russian Federation -IAEA CN-221, EX/P5-24, to be submitted to Nuclear Fusion

27. Loarte et al., Phys. Rev. Letters 83 (18) (1999) 3657.

28. private communication from T. Osborne, DIII-D.

29. C. Silva, 42nd EPS Conference on Plasma Physics, O 1.114, to be submitted to NF